Vehicle System Dynamics

ISSN: 0042-3114 (Print) 1744-5159 (Online) Journal homepage: http://www.tandfonline.com/loi/nvsd20

Hydraulically interconnected vehicle suspension: handling performance

Wade A. Smith , Nong Zhang & William Hu

To cite this article: Wade A. Smith , Nong Zhang & William Hu (2011) Hydraulically interconnected vehicle suspension: handling performance, Vehicle System Dynamics, 49:1-2, 87-106, DOI: 10.1080/00423111003596743

To link to this article: https://doi.org/10.1080/00423111003596743

Published online: 20 Sep 2010.

Vehicle System Dynamics
Vol. 49, Nos. 1–2, January–February 2011, 87–106

Taylor & Francis
Taylor & Francis Group

Hydraulically interconnected vehicle suspension: handling performance

Wade A. Smith, Nong Zhang* and William Hu

Mechatronics and Intelligent Systems, Faculty of Engineering, University of Technology, Sydney, P.O. Box 123, Broadway, NSW 2007, Australia

(*Received 13 March 2009; final version received 19 December 2009; first published 20 September 2010*)

This paper extends recent research on vehicles with hydraulically interconnected suspension (HIS) systems. Such suspension schemes have received considerable attention in the research community over the last few years. This is due, in part, to their reported ability to provide stiffness and damping rates dependent on the suspension mode of operation (i.e. the bounce, roll, pitch or articulation of the unsprung masses relative to the sprung mass), rather than relying on the stiffness and damping characteristics of the single wheel stations. The paper uses a nine-degrees-of-freedom (DOF) vehicle model and simulations of a fishhook manoeuvre to assess the handling performance of a vehicle when it is fitted with: (a) a conventional independent suspension, and (b) an HIS. In the case of the latter, the fluid subsystem is modelled using a nonlinear finite-element approach, resulting in a set of coupled, first-order nonlinear differential equations, which describe the dynamics of the integrated mechanical-hydraulic vehicle system. The simulation results indicate that, in general, the HIS-equipped vehicle possesses superior handling, as measured by the sprung mass roll angle, roll rate, roll acceleration, lateral acceleration and the vehicle's Rollover Critical Factor. The potential effects of the suspension set-up on ride performance are also considered by studying the transient response when one side of the vehicle traverses a half-sine bump. The obtained results are then discussed, and it is shown that they are consistent with previous findings, both by the authors and other researchers. The presented work outlines an alternative approach for studying the dynamics of HIS-equipped vehicles, particularly suited to analyses in the time domain.

Keywords: interconnected suspension; hydraulic system; vehicle dynamics; multi-body dynamics

1. Introduction

Vehicle rollovers are dangerous and potentially fatal events. Certain types of vehicles – such as four wheel drives (4WDs) or sport utility vehicles – are particularly vulnerable to this type of accident, with over one-third of 4WD fatalities involving rollover [1]. Rollovers are complex events, but well-designed suspension systems can greatly reduce vehicular rollover propensity.

Modern vehicle suspensions are required to achieve a number of often conflicting objectives, such as the well-known trade-off between handling stability and ride comfort. A vehicle with a relatively stiff suspension is likely to possess good handling stability but poor ride comfort,

*Corresponding author. Email: nong.zhang@uts.edu.au

ISSN 0042-3114 print/ISSN 1744-5159 online

DOI: 10.1080/00423111003596743
http://www.informaworld.com

and vice versa. One approach to overcoming this compromise is through the use of hydraulic or mechanical interconnections between the individual wheel stations (spring-damper elements).

1.1. *Interconnected suspension*

An *interconnected suspension* system is one in which motion at one wheel station can produce forces at other wheel stations [2]. This is achieved by connecting to one another – either hydraulically or mechanically – the individual spring-damper elements at each wheel. Unlike conventional suspensions – in which modal (i.e. suspension mode-based) stiffness and damping are governed purely by the properties of the single wheel stations – interconnected schemes have the theoretical capability to grant the designer complete control over the stiffness and damping of each suspension mode. In practice, the degree to which individual modes can be controlled depends on the method and exact arrangement of the interconnection employed.

1.2. *Hydraulically interconnected suspension (HIS)*

HIS schemes typically contain, at each wheel station, a single- or double-acting hydraulic cylinder which replaces the conventional shock absorber. The chambers in the cylinders are interconnected by hydraulic circuits, the arrangement of which depends on the objectives of the particular suspension system. Each circuit may comprise elements, such as damper valves, gas-filled accumulators, pipelines, fittings, and flexible hoses.

In HIS systems, relative velocities in the suspension struts cause fluid flows in the circuit(s), which provide energy dissipation. Any flow into or out of the accumulator(s) leads to pressure changes in the circuits and hence to the restoring forces in the suspension strut(s). The hydraulic circuits are arranged such that a nominal flow distribution in a given mode provides the desired levels of stiffness and damping by causing flow into certain dampers and accumulators.

1.3. *Previous research on HISs*

HIS systems were the subject of considerable commercial attention in the 1950s, 1960s and 1970s, when Moulton's Hydrolastic and Hydragas systems were in production. These systems served to improve ride performance by softening the vehicle's pitch and articulation modes relative to the bounce and roll modes [3].

Until quite recently, however, HIS systems have been afforded only sporadic attention in the academic community. In the last five years, however, researchers at The Ohio State University [4,5] and Concordia University [6–9] in particular have shown, both in theory and in practice, the viability of such systems in optimising the ride-handling compromise.

In recent experimental studies by Wilde *et al*., vehicles with HIS systems displayed significantly improved handling capability compared with their non-interconnected 'equivalents' [4,5]. The tests employed therein were based on the fishhook manoeuvre, and it was found that the combination of added roll damping and roll stiffness available with an HIS system was beneficial to the rollover resistance of the vehicle.

More recently, Cao *et al*. [6,9] extended the work of Liu *et al*. [10,11] by studying a vehicle with a pitch plane interconnection. They found that benefits could be obtained by having the freedom to tune the pitch stiffness and damping independently, particularly in heavy vehicle applications.

The present paper intends to build on work previously undertaken by the authors. In earlier work, emphasis was given to the development and use of a linear mechanical-hydraulic system model [12,13] and its experimental verification [14]. However, the fluid subsystem model

used in those studies was frequency-dependent and was thus not readily applicable in the time domain. For this reason, a detailed, nonlinear, finite-element-based fluid system model is used here to conduct time-domain simulations to assess system performance.

1.4. *Layout of paper*

This paper is arranged as follows. The basic vehicle model used throughout the paper is introduced in Section 2, and the relevant equations of motion are given. In Section 3, an HIS system based on the Kinetic H2 suspension is described and the proposed approach for modelling vehicles with HIS is outlined. The chosen fluid component models are discussed and a set of first-order, nonlinear, coupled differential equations, which govern the dynamics of the integrated mechanical-hydraulic vehicle system, is then obtained. The simulation approach is outlined briefly in Section 4, before the results are discussed in Section 5. Suggestions for future work are given in Section 6, and the study's conclusions are drawn in Section 7.

2. Model description and system equations for vehicle with conventional independent suspension

2.1. *Vehicle model*

In this paper, a nine-DOF, lumped-mass full-car model is used, as shown in Figure 1. Typical passenger car parameters, obtained mostly from [15] and outlined in Table 1, are employed. The vehicle consists of a rigid sprung mass (vehicle body), a conventional independent suspension and four unsprung masses (wheel assemblies). The suspension is fitted with front and rear anti-roll bars (not shown in the diagram). The system is assumed to possess linear tyre damping and

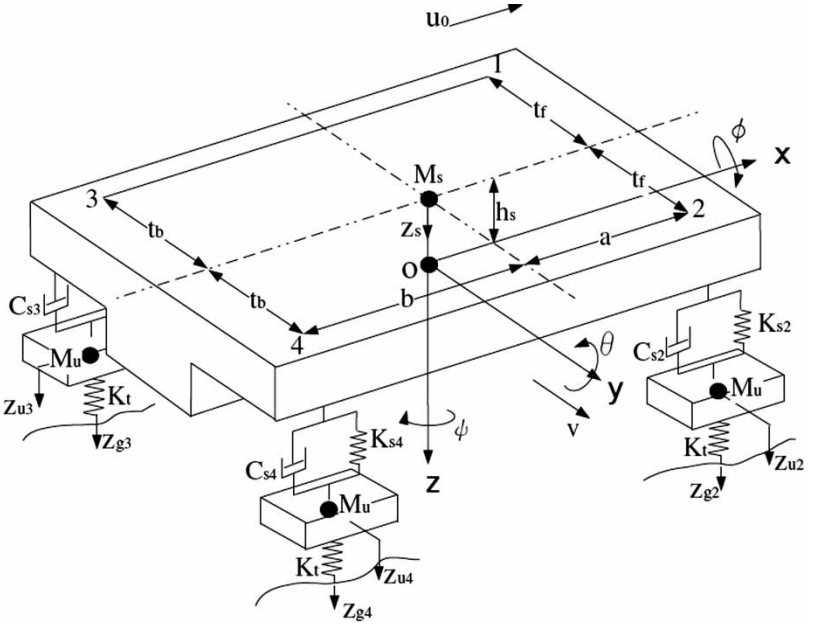

Figure 1. Schematic of the nine-DOF lumped-mass vehicle model with a conventional independent suspension (see Table 1 for parameter values).

Table 1. Properties of the nine-DOF mechanical multi-body subsystem.

Symbol	Value	Units	Description
M_s, M_u	1350/42	kg	Sprung/unsprung mass
I_{xx_s}	380	kg m^2	Sprung mass moment of inertia about the x-axis
I_{yy_s}	1000	kg m^2	Sprung mass moment of inertia about the y-axis
I_{zz_s}	2240	kg m^2	Sprung mass moment of inertia about the z-axis
I_{xz_s}	0	kg m^2	Sprung mass product of inertia about the x–z-axes
$I_{z'z'_u}$	1	kg m^2	Unsprung mass moment of inertia about vertical axis through unsprung mass CG
a	1.253	m	Distance from sprung mass CG to the front axle
b	1.508	m	Distance from sprung mass CG to the rear axle
t_f	0.75	m	Half track width at front of vehicle
t_r	0.75	m	Half track width at rear of vehicle
h_s	0.33	m	Height of sprung mass CG above the roll axis
h_{ra}	0.30	m	Height of roll axis
K_{si}	20	kN m^{-1}	Suspension spring stiffness ($i = 1, 2, 3, 4$)
K_t	200	kN m^{-1}	Tyre spring stiffness
K_{ARBf}	50	kN m rad^{-1}	Front roll bar stiffness
K_{ARBr}	20	kN m rad^{-1}	Rear roll bar stiffness
C_{si}	2000	N s m^{-1}	Suspension damping coefficient (independent suspension only)
C_{si}	0	N s m^{-1}	Suspension damping coefficient (interconnected suspension only)
$c_{\delta\varphi}$	0.07	–	Coefficient for inclination angle to roll angle
$c_{\gamma\varphi}$	0.8	–	Coefficient for rear roll steer angle to roll angle

springing in the vertical direction and linear conventional suspension springing. It is assumed that constraints between the rigid bodies are such that the unsprung masses and the sprung mass translate together in the lateral (y-)direction. In yaw (ψ, rotation about the z-axis), the unsprung masses rotate together with the sprung mass relative to the earth-fixed inertial reference; the roll and pitch rotations (ϕ and θ, respectively), however, are restricted only to the sprung mass.

Under the assumption of a constant forward velocity and the above constraints, the number of DOF of the vehicle model is set to nine: sprung mass lateral and vertical centre-of-mass motions, roll and pitch rotations of the sprung mass about the axis at its CG, yaw rotation for the total vehicle, and four vertical motions of the unsprung masses.

Use is made here of an earth-fixed inertial reference frame, denoted by S_*, and of a vehicle-fixed non-inertial reference frame, S_v, rotating with angular velocity $\vec{\omega}_v = [0, 0, r]^T$ and translating with velocity $\vec{v}_o = [u_0, v, 0]^T$. The equations of motion of the nine-DOF vehicle model were derived by Zhang *et al*. [15]. The state variable vector for this model consists of 18 variables:

$$\mathbf{X}_M(t) = [\mathbf{Z}^T, \dot{\mathbf{Z}}^T]^T \tag{1}$$

in which

$$\begin{aligned} \mathbf{Z} &= [Y_s, Z_s, Z_{u1}, Z_{u2}, Z_{u3}, Z_{u4}, \phi, \theta, \psi]^T \\ \dot{\mathbf{Z}} &= [\dot{Y}_s, \dot{Z}_s, \dot{Z}_{u1}, \dot{Z}_{u2}, \dot{Z}_{u3}, \dot{Z}_{u4}, \dot{\phi}, \dot{\theta}, \dot{\psi}]^T. \end{aligned} \tag{2}$$

After organising the 18 state equations, one obtains the matrix state equations, as follows:

$$\mathbf{T}_M\dot{\mathbf{X}}_M(t) = \mathbf{S}_M\mathbf{X}_M(t) + \mathbf{F}_M(t), \tag{3}$$

where

$$\mathbf{T}_M = \begin{bmatrix} \mathbf{I} & \mathbf{0} \\ \mathbf{0} & \mathbf{M} \end{bmatrix}_{18\times18} \quad \mathbf{S}_M = \begin{bmatrix} \mathbf{0} & \mathbf{I} \\ -\mathbf{K} & -\mathbf{C} \end{bmatrix}_{18\times18} \quad \mathbf{F}_M(t) = \begin{bmatrix} \mathbf{0} \\ \mathbf{F}_m(t) \end{bmatrix}_{18\times1}.$$

The roll moment for this vehicle model is calculated using $\sum M_x = \dot{H}_x - r H_y$, as outlined in [15]. H refers to the angular momentum about the given axis (see Figure 1).

2.2. *Tyre model*

The tyre model used in this paper is a version of Pacejka's Magic-Formula (MF) model, as described in [16]. The model's input variables are the vertical tyre force, the longitudinal and lateral slip angles and the inclination angle. The output variables are the longitudinal and lateral tyre forces and the self-aligning moment at the tyre contact patch. The interested reader is referred to Zhang *et al*. [15], where an application of the MF tyre model is described in greater detail.

3. Model description and system equations for vehicle with HIS

3.1. *Model description and HIS operation*

The second vehicle model used in this paper employs an HIS system; the mass, inertia and spring stiffness values are identical to those described above, but the conventional suspension's shock absorbers are replaced by the HIS system's double acting cylinders. The model for the HIS-equipped vehicle thus contains two subsystems: one mechanical and one hydraulic. The completely passive hydraulic subsystem is based on the H2 suspension system, designed by Kinetic Pty Ltd [17]. The hydraulic layout features right–left symmetry and two identical fluid circuits, as shown in Figure 2. Also included in the fluid system are: two nitrogen-filled, diaphragm-type accumulators; interconnecting pipelines; ten damper valves, which provide

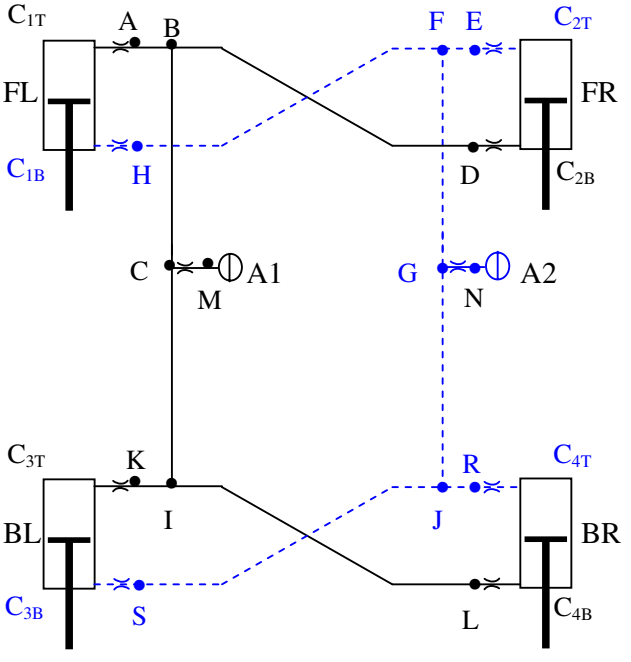

Figure 2. Layout of the hydraulic subsystem used in the HIS-equipped vehicle model (see Table 2 for parameter values).

Table 2. Properties of the hydraulic subsystem.

Symbol	Value	Units	Description
System properties			
$\bar{P}$	1.5	MPa	Mean system pressure
Hydraulic oil properties			
ρ	870	$\mathrm{kg\,m^{-3}}$	Density
μ	0.05	$\mathrm{N\,s\,m^{-2}}$	Viscosity
β_{oil}	1400	MPa	Bulk modulus
Pipeline dimensions			
l_{AB}, l_{EF}	1.0	m	Length of pipe from A to B and from E to F
l_{BC}, l_{FG}	1.6	m	Length of pipe from B to C and from F to G
l_{CI}, l_{GJ}	1.6	m	Length of pipe from C to I and from G to J
l_{BD}, l_{FH}	1.0	m	Length of pipe from B to D and from F to H
l_{KI}, l_{RJ}	1.0	m	Length of pipe from K to I and from R to J
l_{IL}, l_{JS}	1.0	m	Length of pipe from I to L and from J to S
d_{p}	1.0×10^{-2}	m	Pipeline diameter
Accumulator properties			
V_{p}	3.2×10^{-4}	$\mathrm{m^3}$	Pre-charge gas volume
P_{p}	0.5	MPa	Pre-charge pressure
Double-acting cylinder properties			
D_{C}, D_{R}	0.022, 0.0095	m	Diameter of cylinder and piston rod
x_{s}	0.15	m	Stroke length
Damper valve loss coefficients			
$R_{V_{\mathrm{C}}}$	5×10^9	$\mathrm{kg\,s^{-1}\,m^{-4}}$	Linear loss coefficient for cylinder valves
$R_{V_{\mathrm{A}}}$	3.2×10^9	$\mathrm{kg\,s^{-1}\,m^{-4}}$	Linear loss coefficient for accumulator valves

the desired levels of damping in various suspension modes; and four double-acting hydraulic cylinders, which typically reside in the space formerly occupied by the shock absorbers [5]. Table 2 shows the parameters relating to the hydraulic subsystem; all of the mechanical subsystem parameters defined in Table 1 (other than those relating to the shock absorbers) are also used in the HIS-equipped vehicle.

The H2 system (and HIS systems more broadly) works by distributing fluid flow to dampers and accumulators in a way that depends on the particular suspension mode in operation (i.e. bounce, roll, pitch or articulation). In the bounce mode, when all of the cylinders are in compression (or extension), fluid flows out of each cylinder's top chamber. Most of the displaced fluid will flow into the laterally opposed cylinder's bottom chamber. But owing to the piston rod, the bottom chamber has a slightly smaller swept volume. Thus a small volume of fluid – the rod volume – will flow instead into (or out of, during the extension phase) the accumulator. Thus, the accumulators and accumulator dampers should have a small effect on the bounce mode.

In the roll mode, every chamber in one circuit has fluid flowing into it, while every chamber in the other circuit has fluid flowing out. The only place for the displaced fluid to come from/go to is the accumulator. Thus, the accumulator and accumulator dampers have a very significant effect on the roll mode. In the pitch and warp modes, there is no fluid flow into or out of the accumulators. Thus, the accumulators and accumulator dampers have no nominal effect on these modes. Another point of note is that the cylinder dampers affect every mode significantly.

3.2. *Basic system equations*

From [12], we note that the equation of motion for the integrated mechanical-hydraulic system can be written in the form:

$$\mathbf{M}\ddot{\mathbf{Z}}(t) + \mathbf{C}\dot{\mathbf{Z}}(t) + \mathbf{K}\mathbf{Z}(t) = \mathbf{D}_1\mathbf{A}\mathbf{P}(t) + \mathbf{F}_{\mathbf{ext}}(t), \tag{4}$$

where the displacement vector, **Z**, is as defined in the previous section; $\mathbf{D}_1\mathbf{AP}$ describes the forces in the cylinders due to hydraulic pressure; **M**, **C** and **K** are the mass, damping and stiffness matrices, respectively; $\mathbf{F_{ext}}$ refers to any external forces exerted on the mechanical subsystem other than those from the hydraulic subsystem; and $\mathbf{D}_1$ is a linear transformation matrix. The area matrix, **A**, and pressure vector, **P**, relate to the corresponding cylinder chambers (T – top; B – bottom) and are defined as follows:

$$\mathbf{A} = \mathrm{diag}(A_{\mathrm{T}}^{C1}, A_{\mathrm{B}}^{C1}, A_{\mathrm{T}}^{C2}, A_{\mathrm{B}}^{C2}, A_{\mathrm{T}}^{C3}, A_{\mathrm{B}}^{C3}, A_{\mathrm{T}}^{C4}, A_{\mathrm{B}}^{C4})$$
$$\mathbf{P} = [P_{\mathrm{T}}^{C1}, P_{\mathrm{B}}^{C1}, P_{\mathrm{T}}^{C2}, P_{\mathrm{B}}^{C2}, P_{\mathrm{T}}^{C3}, P_{\mathrm{B}}^{C3}, P_{\mathrm{T}}^{C4}, P_{\mathrm{B}}^{C4}]^{\mathrm{T}}.$$

3.3. *Mechanical-hydraulic system boundary conditions*

The cylinder chambers form the boundary between the mechanical and hydraulic subsystems. The compressibility of the hydraulic fluid in each of the cylinder chambers is taken into account by the well-known relation for fluid compressibility:

$$Q_{\mathrm{comp}} = \frac{V}{\beta}\frac{\mathrm{d}P}{\mathrm{d}t}, \tag{5}$$

where V and β are the volume and effective bulk modulus of the cylinder chamber.

Thus the fluid compressibility in the top and bottom chambers is given by

$$\begin{aligned} Q_{\mathrm{comp}_{(\mathrm{T})}} &= \dot{Z}_{\mathrm{s\text{-}u}}(t)A_{\mathrm{T}} - Q_{\mathrm{T}}(t) = \frac{V_{\mathrm{T0}} - Z_{\mathrm{s\text{-}u}}(t)A_{\mathrm{T}}}{\beta_{\mathrm{oil}}}\dot{P}_{\mathrm{T}}(t) \\ Q_{\mathrm{comp}_{(\mathrm{B})}} &= Q_{\mathrm{B}}(t) - \dot{Z}_{\mathrm{s\text{-}u}}(t)A_{\mathrm{B}} = \frac{V_{\mathrm{B0}} + Z_{\mathrm{s\text{-}u}}(t)A_{\mathrm{T}}}{\beta_{\mathrm{oil}}}\dot{P}_{\mathrm{B}}(t) \end{aligned}, \tag{6}$$

where Q_{T} and Q_{B} denote the volume flow rates where the pipeline meets the top and bottom cylinder chamber, respectively; $\dot{P}_{\mathrm{T}}$ and $\dot{P}_{\mathrm{B}}$ are the rates of change of the in-chamber pressure; V_{T0} and V_{B0} are the original (equilibrium) volumes of the top and bottom cylinder chambers; and $Z_{\mathrm{s\text{-}u}}$ is the displacement in the suspension strut, which is equal to the relative displacement between the unsprung mass and the point of strut contact on the sprung mass.

When applied to all eight chambers in the fluid subsystem in Figure 2, Equation (6) can be written in terms of the flow vector $\mathbf{Q} = [Q_{\mathrm{T}}^{C1}, Q_{\mathrm{B}}^{C1}, Q_{\mathrm{T}}^{C2}, Q_{\mathrm{B}}^{C2}, Q_{\mathrm{T}}^{C3}, Q_{\mathrm{B}}^{C3}, Q_{\mathrm{T}}^{C4}, Q_{\mathrm{B}}^{C4}]^{\mathrm{T}}$ as follows:

$$\mathbf{Q}(t) = \mathbf{A}\mathbf{D}_2\dot{\mathbf{Z}}(t) + \tilde{\mathbf{V}}(t)\dot{\mathbf{P}}(t) \tag{7}$$

in which $\tilde{\mathbf{V}}$ is a time-variant matrix of cylinder volume and bulk modulus terms, and $\mathbf{D}_2$ is a constant linear transformation matrix.

3.4. *Fluid component models*

The models used for each fluid subsystem component are as follows.

Damper valves: The damper valves play an important role in the HIS system, and they usually possess nonlinear pressure-flow characteristics. The study of damper flow dynamics is a specialised subject, generally involving geometrically small flow paths and, consequently, advanced modelling techniques. Such an investigation is beyond the scope of this paper; the interested reader is instead referred to [18] for further information. The simplified model used

here assumes that the damper valves have negligible fluid volume and involve linear pressure losses, as follows:

$$Q_{\mathrm{v}} = \frac{1}{R_{\mathrm{v}}}(P_{\mathrm{in}} - P_{\mathrm{out}}). \tag{8}$$

Pipelines: A lumped parameter model of the fluid pipelines is developed by dividing them into several elements. The mean pressure and mean flow in each element is assumed as an arithmetic mean of the pressure and flow rate at both ends of the pipe. The fluid flow in the pipe is assumed to be a one-dimensional compressible flow to accommodate the water hammer phenomenon. Assuming the pressure losses due to viscosity are proportional to the mean flow rate, and the magnitude of losses is the same as the inertia and pressure forces, the momentum equation can be written as

$$\frac{\rho l_i}{A_i}\dot{Q}_i = (P_{i1} - P_{i2}) - R_i l_i Q_i, \tag{9}$$

where $R_i = 8\pi\rho/A_i^2$ is the viscous loss coefficient, ρ is the fluid density, l_i the pipe length, and A_i the pipe section area.

The continuity equation for the pipeline is written in terms of the mean pressure and flow difference between the ends of the pipe element, as follows:

$$\dot{P}_i = \frac{\beta}{\tilde{V}_i}(Q_{i1} - Q_{i2}), \tag{10}$$

where β, the effective pipe-fluid bulk modulus, is treated as a constant. The mean pressure and mean flow rate of each pipe element are given as the arithmetic mean of the pressure and flow at the ends of the element, respectively,

$$P_i = \frac{1}{2}(P_{i1} + P_{i2}) \quad \text{and} \quad Q_i = \frac{1}{2}(Q_{i1} + Q_{i2}). \tag{11}$$

Equations (9)–(11) apply to each pipe element; combining them results in a set of coupled first-order differential equations that govern the pressure and flow at defined nodal points in the fluid circuits. In general, aside from the system boundaries, one pressure and one flow term for each line element are required in the state vector in order to fully describe the system state.

Cylinder chambers: As mentioned previously, the cylinder chambers are treated as ideal capacitive elements. This is a special case of the line model, with Equation (9) ignored. The length (and hence, volume) of the cylinder chambers varies as the sprung and unsprung masses move relative to one another. This volume change creates a coupling nonlinearity between the mechanical and hydraulic subsystems.

Accumulators: The accumulators are modelled by assuming an adiabatic process. The pressure and volume at any time in the accumulator – P_{a} and V_{a}, respectively – are related to the pre-charge values, P_{p} and V_{p}, as follows:

$$P_{\mathrm{a}} V_{\mathrm{a}}^{\gamma} = P_{\mathrm{p}} V_{\mathrm{p}}^{\gamma} = \text{constant}, \tag{12}$$

where γ is the ratio of specific heats for the gas. The compressibility of the oil in the accumulator is neglected, as the oil stiffness is much greater than that of the nitrogen contained in the bladder. The adiabatic gas law is used to model the accumulator pressure as a function of gas

volume at the precharged pressure. Taking the partial time derivative of Equation (12), and noting that the flow into the accumulator is given by $Q_\mathrm{a} = -\partial V_\mathrm{a}/\partial t$, the pressure gradient of the accumulator can be written as a nonlinear function of pressure, i.e.

$$\dot{P}_\mathrm{a} = \frac{\gamma Q_\mathrm{a} P_\mathrm{a}}{V_\mathrm{p}} \left(\frac{P_\mathrm{a}}{P_\mathrm{p}}\right)^{1/\gamma}. \tag{13}$$

3.5. *Fluid subsystem model*

To obtain the fluid subsystem equations, the fluid lines are meshed into a number of finite elements, before applying Equation (7) and each of the above fluid component models. At each end node of each hydraulic element, the fluid outflow rate of the upstream element is equal to the inflow rate of the neighbouring downstream element. At a junction node, the net inflow is equal to the net outflow, and the pressures (for different fluid elements) are the same. Because of these physical constraints, not every element requires a pressure and flow term in the state vector: some of these terms relating to the internal nodes can be eliminated, and flow rates at the boundary nodes can be determined from the relative motion of the rigid bodies.

This results in a set of coupled, nonlinear first-order differential equations governing the pressure and flow at defined nodal points in the fluid circuits. The equations are in the following form:

$$\mathbf{G}_1(t)\dot{\mathbf{X}}_\mathrm{H}(t) + \mathbf{G}_2\dot{\mathbf{X}}_\mathrm{H}(t) = \mathbf{G}_3(t)\dot{\mathbf{Z}}(t) + \mathbf{G}_4(t)\mathbf{X}_\mathrm{H}(t) + \mathbf{G}_5\mathbf{X}_\mathrm{H}(t) \tag{14}$$

in which the hydraulic subsystem state vector, $\mathbf{X}_\mathrm{H}$, includes the pressure terms relating both to the end nodes of the fluid circuits and to k internal nodes, as well as the flow terms relating to m internal nodes:

$$\mathbf{X}_\mathrm{H}(t)_{(8+n)\times 1} = [\mathbf{P}, P_{\mathrm{int}_1}, P_{\mathrm{int}_2}, \ldots, P_{\mathrm{int}_k}, Q_{\mathrm{int}_1}, Q_{\mathrm{int}_2}, \ldots, Q_{\mathrm{int}_m}]^\mathrm{T}, \tag{15}$$

where $n = k + m$. The value of n depends on the fluid subsystem's finite element mesh, which is determined by the desired accuracy of the solution and the particular hydraulic layout. A higher number of finite elements mean that higher frequency phenomena are captured in the simulation. In the simulations performed in this paper, a total of 34 state variables are used ($k = 16$, $m = 10$), as follows:

$$\begin{aligned}\mathbf{P}_\mathrm{int} = [&P_\mathrm{A}^{AB}, P_\mathrm{B}^{AB}, P_\mathrm{M}^{A1}, P_\mathrm{C}^{BC}, P_\mathrm{I}^{CI}, P_\mathrm{L}^{IL}, P_\mathrm{E}^{EF}, P_\mathrm{F}^{EF}, P_\mathrm{N}^{A2}, P_\mathrm{G}^{FG}, P_\mathrm{J}^{GJ},\\ &P_\mathrm{S}^{JS}, P_\mathrm{B}^{C3}, P_\mathrm{D}^{CD}, P_\mathrm{K}^{KI}, P_\mathrm{H}^{GH}, P_\mathrm{R}^{RJ}]^\mathrm{T}\\ \mathbf{Q}_\mathrm{int} = [&Q_\mathrm{B}^{AB}, Q_\mathrm{C}^{BC}, Q_\mathrm{C}^{CI}, Q_\mathrm{I}^{CI}, Q_\mathrm{I}^{IL}, Q_\mathrm{F}^{EF}, Q_\mathrm{G}^{FG}, Q_\mathrm{G}^{GJ}, Q_\mathrm{J}^{GJ}, Q_\mathrm{J}^{JS}]^\mathrm{T}\end{aligned}, \tag{16}$$

in which the superscripts denote the relevant hydraulic element: two letters represents a pipeline element; the letter A followed by a number represents an accumulator. The subscripts define the specific location.

After rearranging the 34 state equations, one obtains the fluid subsystem equations, as follows:

$$\mathbf{T}_\mathrm{H}\dot{\mathbf{X}}_\mathrm{H}(t) = \mathbf{S}_\mathrm{H}\mathbf{X}_\mathrm{H}(t) + \mathbf{F}_\mathrm{H}(t), \tag{17}$$

where $\mathbf{T}_{\mathrm{H}_{34\times 34}} = \mathbf{G}_2$ and $\mathbf{S}_{\mathrm{H}_{34\times 34}} = \mathbf{G}_5$. The time-dependent coefficients – $\mathbf{G}_1$, $\mathbf{G}_3$ and $\mathbf{G}_4$ – are captured in the $\mathbf{F}_\mathrm{H}$ term.

3.6. *Complete integrated vehicle equations*

Equations (3), (4) and (17) can be combined to obtain the equations of motion for the complete integrated vehicle, as follows:

$$\mathbf{T}\dot{\mathbf{X}}(t) = \mathbf{S}\mathbf{X}(t) + \mathbf{F}(t), \tag{18}$$

where

$$\mathbf{T} = \begin{bmatrix} \mathbf{I} & \mathbf{0} & \mathbf{0} \\ \mathbf{0} & \mathbf{M} & \mathbf{0} \\ \mathbf{0} & \mathbf{0} & \mathbf{T}_{\mathrm{H}} \end{bmatrix}_{52\times 52} \quad \mathbf{S} = \begin{bmatrix} \mathbf{0} & \mathbf{I} & \mathbf{0} \\ -\mathbf{K} & -\tilde{\mathbf{C}} & \mathbf{S}_{\mathrm{H2M}} \\ \mathbf{0} & \mathbf{0} & \mathbf{S}_{\mathrm{H}} \end{bmatrix}_{52\times 52} \quad \mathbf{F}(t) = \begin{bmatrix} \mathbf{0} \\ \mathbf{F}_{\mathrm{m}}(t) \\ \mathbf{F}_{\mathrm{H}}(t) \end{bmatrix}_{52\times 1}.$$

The state vector is $\mathbf{X}(t)_{52\times 1} = [\mathbf{Z}^{\mathrm{T}}, \dot{\mathbf{Z}}^{\mathrm{T}}, \mathbf{X}_{\mathrm{H}}]^{\mathrm{T}}$, and $\mathbf{S}_{\mathrm{H2M}} = [(\mathbf{D}_1\mathbf{A})_{9\times 8}, \mathbf{0}_{9\times 26}]$. The original damping matrix from Equation (3) is modified to $\tilde{\mathbf{C}}$ by removing the coefficients relating to the conventional shock absorbers. The $\mathbf{F}_{\mathrm{m}}$ term accounts for any external forces such as road input exerted on the mechanical subsystem, and $\mathbf{F}_{\mathrm{H}}$ describes both the nonlinear coupling between the mechanical and hydraulic subsystems as well as any nonlinear effects in the fluid subsystem itself.

Equation (18) can be converted to the more conventional state-space form by pre-multiplying $\mathbf{T}^{-1}$:

$$\dot{\mathbf{X}}(t) = \mathbf{A}\mathbf{X}(t) + \mathbf{B}\mathbf{U}(t), \tag{19}$$

where $\mathbf{A} = \mathbf{T}^{-1}\mathbf{S}$, $\mathbf{B} = \mathbf{T}^{-1}$ and $\mathbf{U}(t) = \mathbf{F}(t)$. Equation (19) is used to obtain the results in the following sections.

4. Simulation approach

4.1. *Application of the system equations*

In the ensuing simulations, at time 0, the system is in static equilibrium and the initial system state can be determined from static force-balancing equations. At the next instant, the disturbances from the specified inputs are applied to the system, so the dynamic state of the integrated system is determined from the state-space system model (Equation (19)), combining the dynamics of the rigid body system and the suspension fluid circuits. A fourth-order Runge–Kutta numerical integration method is used to solve the set of differential equations.

Simulations for the vehicle with conventional independent suspension (Equation (3)) are also provided for comparison.

4.2. *Steering input*

In the first set of simulations used in this paper, the vehicles are subjected to the well-known fishhook manoeuvre [19]. The steering input is applied to both models under the same conditions: the vehicle velocity is 75 km/h and the maximum steering angle is 270°. Figure 3 shows the applied steering wheel angle input as a function of time.

The performance measures studied for this input include the vehicle roll angle, roll velocity, roll acceleration and lateral acceleration, all of which are desirable to minimise. The first four measures are generally considered indicators of a vehicle's handling capability, while the remainder are indicative of ride performance.

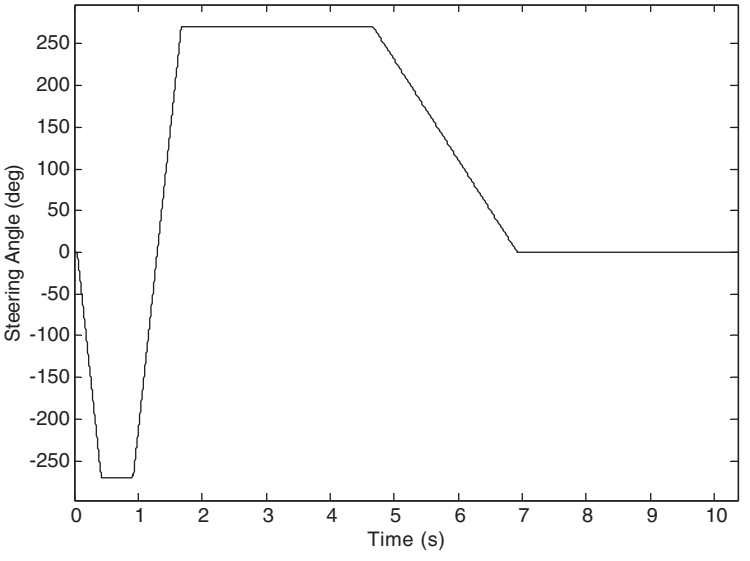

Figure 3. Steering angle input.

In addition to these measures, the Rollover Critical Factor (RCF) is also considered in this study. The RCF quantifies the rollover resistance capability of a light vehicle. It is defined as follows:

$$\mathrm{RCF}(t) = g\left[\frac{t_\mathrm{f} + t_\mathrm{r}}{2} - h_\mathrm{s}|\phi(t)|\right] - |a_y(t)|[(h_\mathrm{s} + h_\mathrm{ra}) - Z_\mathrm{s}(t)] - \frac{I_{xx_\mathrm{s}}|\ddot{\phi}(t)|}{M_\mathrm{s}}, \tag{20}$$

where a_y is the vehicle lateral acceleration and g is the acceleration due to gravity; the other terms are defined in Figure 1 and Table 1. A smaller RCF value indicates lower rollover resistance capability; rollover will occur when the RCF value becomes negative.

4.3. *Half-sine bump input*

In the second set of simulations used in this paper, the vehicles are subjected to a half-sine bump input applied to the left-side wheels only. The bump is applied to both models under the same conditions: the vehicle velocity is 20 km/h, the maximum bump height is 0.08 m and the front tyre first strikes the bump at $t = 1.0$ s. Figure 4 shows the half-sine bump as a function of distance.

The performance measures studied for this input include the vehicle bounce, bounce acceleration, roll angle, roll acceleration, pitch angle and pitch acceleration responses, all of which are desirable to minimise.

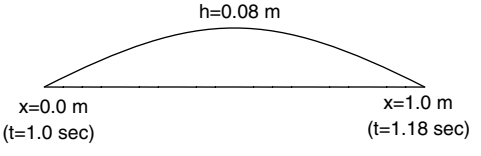

Figure 4. Half-sine bump input.

5. Results and discussion

5.1. *Fishhook turn*

The responses for the Kinetic-equipped and independent suspension vehicles undergoing the fishhook manoeuvre are displayed in Figures 5–9. It is clear from the plots that the vehicle with

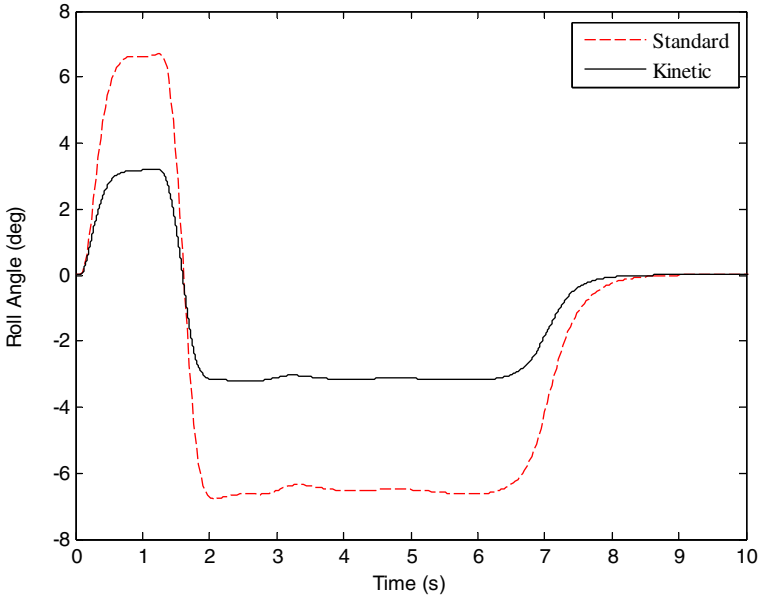

Figure 5. Vehicle roll angle response to fishhook manoeuvre.

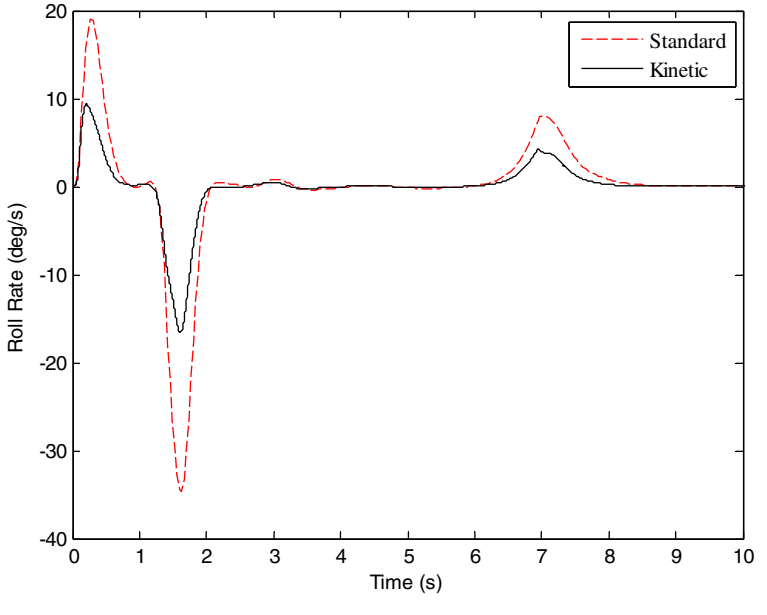

Figure 6. Vehicle roll rate response to fishhook manoeuvre.

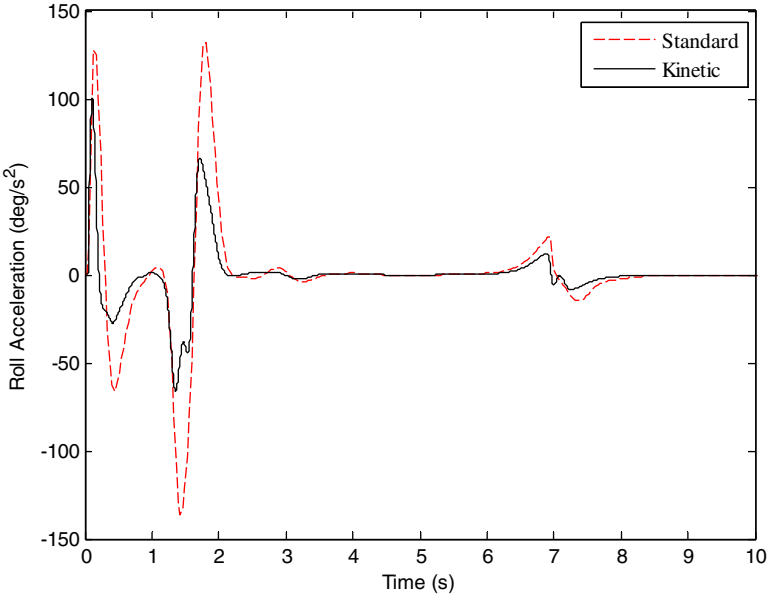

Figure 7. Vehicle roll acceleration response to fishhook manoeuvre.

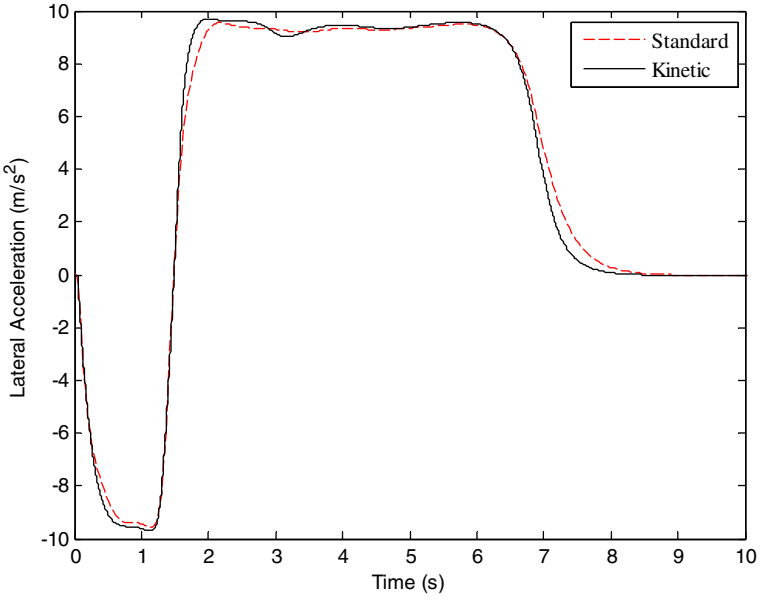

Figure 8. Vehicle lateral acceleration response to fishhook manoeuvre.

the Kinetic suspension experiences a significantly smaller roll response, indicating superior handling. This is likely due to the added roll stiffness provided by the interconnection scheme, which acts as an anti-oppositional system in the roll plane [20,21]. This is consistent with results previously obtained by the authors via free vibration analysis [12]. With the parameters employed, the anti-roll bars fitted to the independent suspension evidently provide much lower roll stiffness than that provided by the Kinetic system.

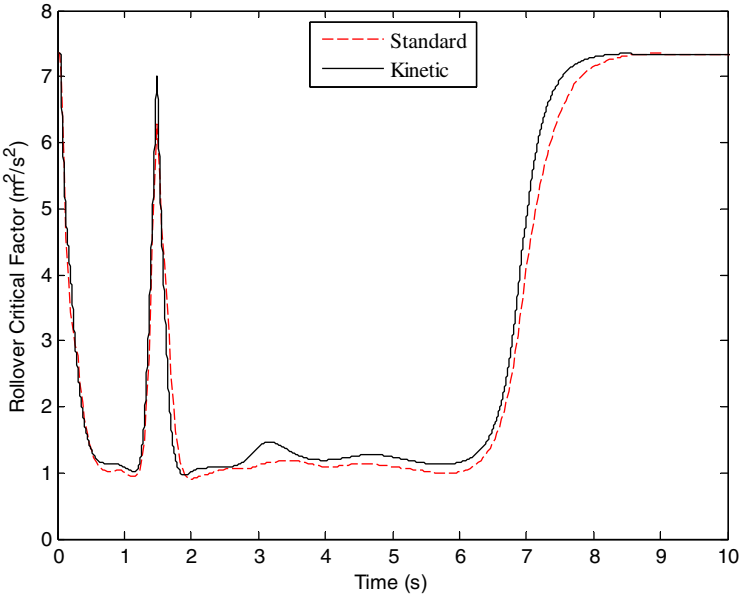

Figure 9. Vehicle RCF during fishhook manoeuvre.

The lateral acceleration, on the other hand, does not appear to be drastically affected by the addition of the interconnected suspension. This indicates that the major component of the lateral acceleration in this simulation is the rigid-body vehicle mode, owing to the curvature of the vehicle's path. This finding is consistent with that of Wilde *et al*. [5], who found in their experimental fishhook study that a Kinetic-equipped vehicle was able to trace a path of tighter curvature than an equivalent independently suspended vehicle, and thus the lateral acceleration for the two vehicles was comparable throughout the manoeuvre.

Taking into account these factors, we can see from Figure 9 that the RCF curves for the two vehicles are not markedly different, although the standard vehicle does exhibit lower rollover resistance in the critical low-RCF region. It is noted that the numerical value of the lateral acceleration term in the RCF equation (Equation (20)) is, throughout most of the manoeuvre, much larger than the terms associated with the roll angle and roll acceleration. Thus, the reduced roll response achieved with the Kinetic suspension leads to only moderate improvements in the RCF. This suggests a need to consider a multitude of indicators in assessing vehicle handling performance, rather than relying on, say, the RCF indicator alone.

5.2. *Half-sine bump*

Looking at Figures 10–15, it is noted that in comparison to the independent suspension, the Kinetic vehicle experiences a slightly larger response in the bounce mode, which is only slightly stiffened by the interconnected suspension. This is due to the unequal areas of the top and bottom of the piston in the double-acting cylinders, creating a small amount of 'accumulator flow' in the bounce mode [12].

In the roll mode, the Kinetic vehicle displays a significantly larger response, suggesting that there is a ride penalty associated with substantially stiffening that mode.

The two vehicles display reasonably similar characteristics in the pitch mode, although the Kinetic-equipped vehicle exhibits a slightly higher level of damping. The similarity in the responses is due to the fact that the Kinetic system does not alter the stiffness of the pitch

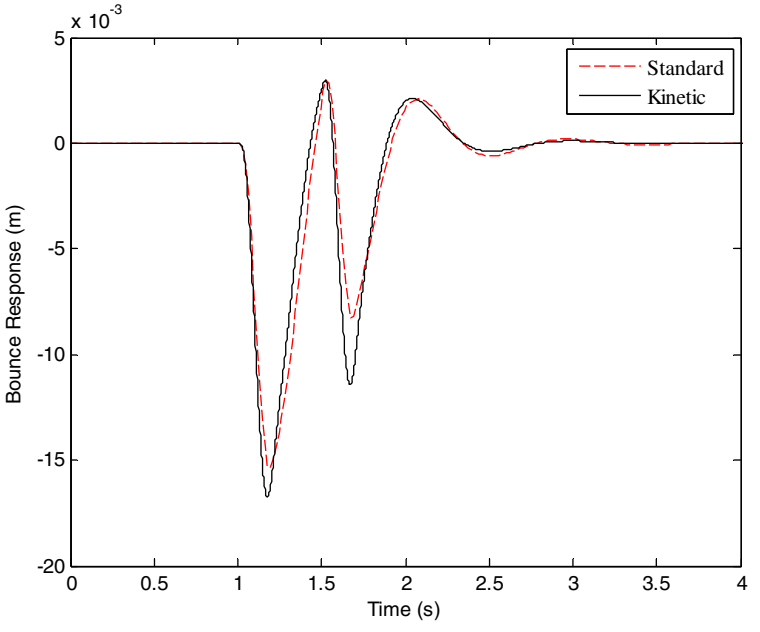

Figure 10. Vehicle bounce response to half-sine bump input.

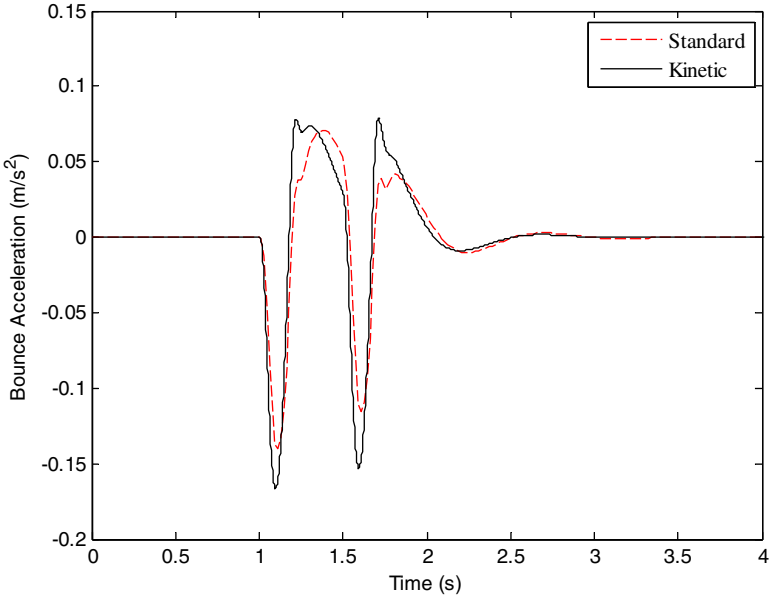

Figure 11. Vehicle bounce acceleration response to half-sine bump input.

mode: the nominal flow distribution in the pitch consists of fore-and-aft flow between the front and rear cylinder chambers. This lack of any 'accumulator flow' means that there is no additional air-spring effect added to the pitch mode, and hence no added stiffness.

In summary, there appears to be moderate negative implications for ride comfort associated with the Kinetic suspension. This is due mostly to the substantially increased roll stiffness that it provides.

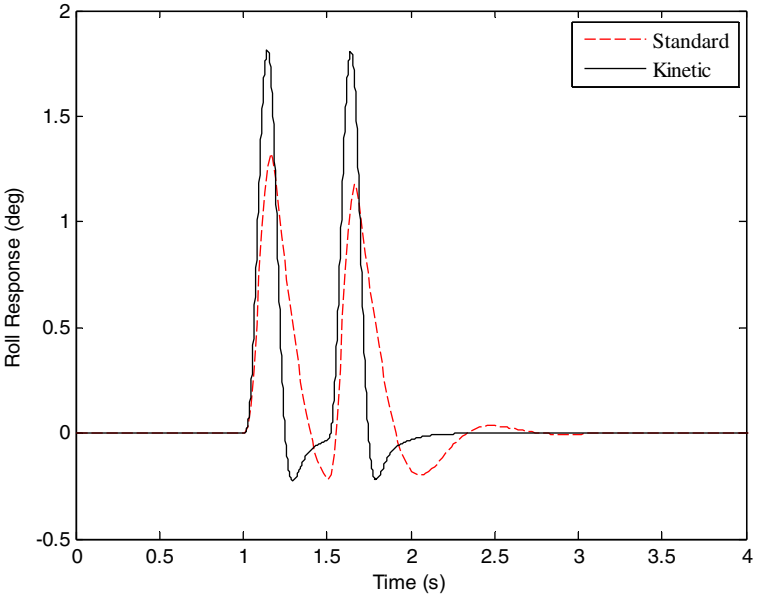

Figure 12. Vehicle roll response to half-sine bump input.

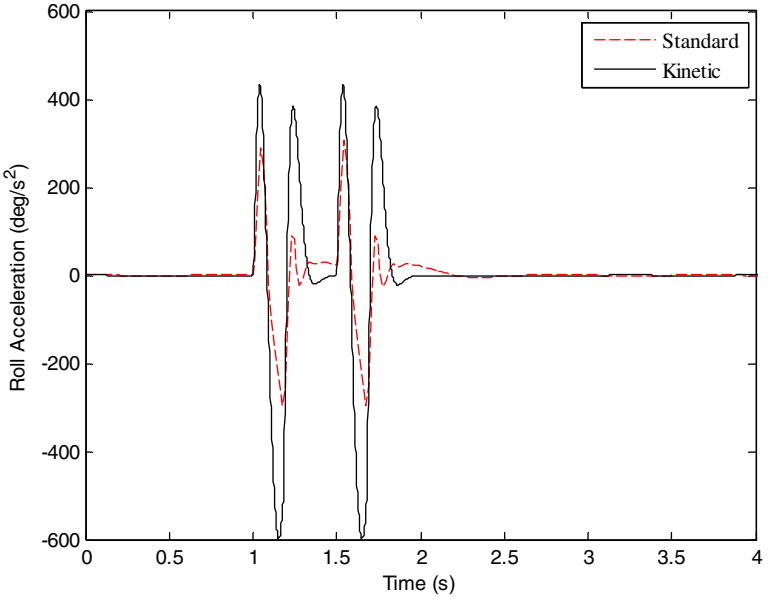

Figure 13. Vehicle roll acceleration response to half-sine bump input.

6. Further discussions and future work

6.1. *Limitations and future work*

Owing to its nonlinearity, the presented model requires considerable computational time to run (∼60 min for the fishhook turn and ∼20 min for the bump input, performed on a Linux cluster using a high-speed 3.2 GHz quad-core processor). It has been found previously that

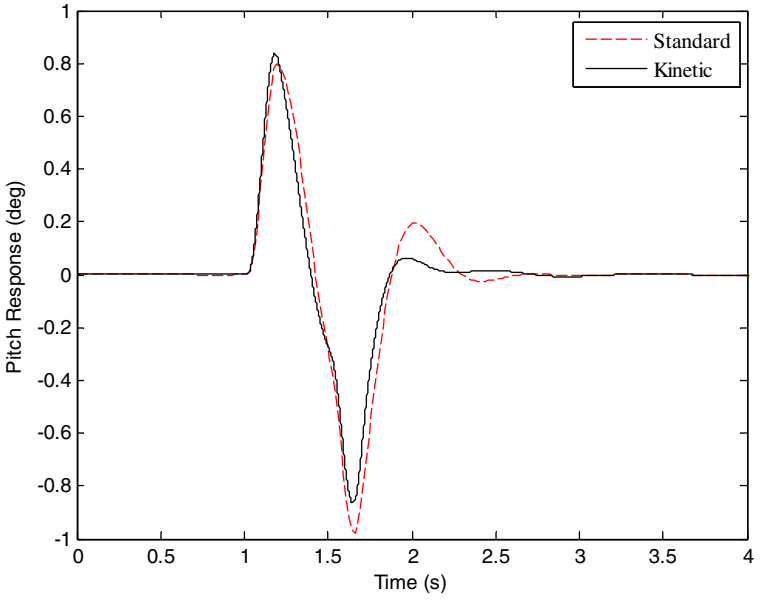

Figure 14. Vehicle pitch response to half-sine bump input.

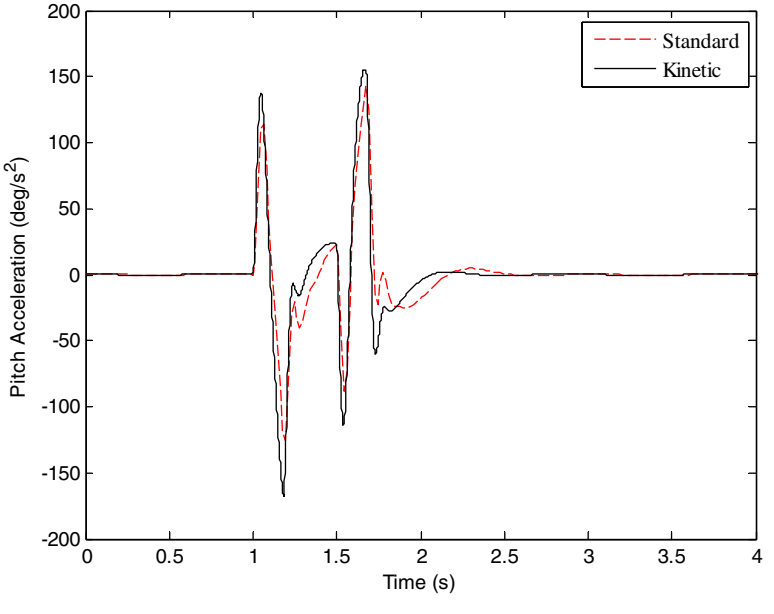

Figure 15. Vehicle pitch acceleration response to half-sine bump input.

using a linear approach to model the Kinetic suspension system may be applicable in a number of small-to-moderate amplitude applications ($\pm$1.5 to 3 mm) [21], but further work remains to be done in that regard. In particular, there remains the need to model the damper valves in more detail. Typical suspension dampers comprise a three-stage valve operation, with different damping properties in the compression and rebound directions. Thus, the applicability of the linear pressure loss model requires further investigation. Detailed CFD modelling may be required for that task [18].

There may also be some value in determining when fluid compressibility must be taken into account and when it can be disregarded. The authors have found that while the fluid-system-dominated natural frequencies might be as high as 180 Hz in an HIS-equipped half-car with rigid pipelines, those natural frequencies drop substantially in the context of a full-car (requiring longer pipelines) with more compliant lines (e.g. soft hoses instead of pipes) [22]. In such cases, the fluid-system-dominated modes can be well below 50 Hz, and they begin to play a role in ride performance. In addition, there remains a concern over fluid-borne noise issues in HIS systems, and to capture this phenomenon requires a significant level of detail in the modelling [23]. Ultimately, the modelling of fluid compressibility – and the use of the finite element approach more broadly – becomes increasingly justifiable as the fluid system becomes more compliant and the frequency range of interest moves further up the frequency band.

Possible further work could also include simulating a greater number of vehicle manoeuvres/inputs and optimising the system's input parameters.

7. Conclusions

This paper has presented an alternative approach for modelling vehicles fitted with a general HIS system. The fluid subsystem is modelled using first-order nonlinear differential equations, so a time-domain solver must be employed in the simulations.

The methodology is applied to a vehicle equipped with a Kinetic H2 interconnected system. The vehicle response is simulated while undergoing the well-known fishhook manoeuvre and while driving over a half-sine bump. The response of an identical vehicle fitted instead with a conventional independent suspension is also simulated. The obtained results show that, in terms of the common rollover resistance measures, the Kinetic vehicle performs well in the fishhook turn, suggesting good handling performance. On the other hand, the results from the bump input simulations suggest there is a moderate reduction in ride comfort associated with the increased roll stiffness provided by the Kinetic suspension.

The findings of the paper suggest that while interconnected suspension schemes can provide much greater flexibility to specify modal stiffness and damping parameters independently (e.g. greatly increased roll stiffness without affecting bounce stiffness) – a characteristic unique among passive suspensions – there is a limit to the benefits that can be expected from such a characteristic. Exploring these limits further is an area recommended for future studies.

Acknowledgements

The financial support of this work by the Australian Research Council (ARC LP0562440) and the University of Technology, Sydney, is gratefully acknowledged.

Notation

a_y	lateral acceleration of the sprung mass centre of gravity (CG)
A_j^{Ci}	area of piston in j (top/bottom) part of cylinder i, $\quad i = 1, 2, 3, 4$
h_{ra}	height of roll axis
h_{s}	height of sprung mass CG above the roll axis
$H_{x/y/z}$	angular momentum about given axis
$I_{xx_{\mathrm{s}}}$	sprung mass moment of inertia about the x-axis
l	length of pipeline

M_{s}	vehicle sprung mass
$M_{x/y/z}$	moment about given axis
P_j^{Ci}	hydraulic pressure at surface of piston in j (top/bottom) part of cylinder i
Q	volumetric flow rate
r	yaw rate of the complete vehicle
R	viscous pressure loss coefficient
t	time
t_{f}	half track width at front of vehicle
t_{r}	half track width at rear of vehicle
u_0	constant longitudinal velocity of the sprung mass CG
v	Lateral velocity of the sprung mass CG
V	volume
Y_{s}	lateral displacement of the sprung mass CG
Z_{s}	vertical displacement of the sprung mass CG
$Z_{\mathrm{s\text{-}u}}$	suspension strut displacement
$Z_{\mathrm{u}i}$	vertical displacement of the unsprung masses
β	pipe-fluid bulk modulus
β_{oil}	fluid bulk modulus
γ	ratio of specific heats for gas in accumulator
θ	pitch angle of the sprung mass
ρ	fluid density
ϕ	roll angle of the sprung mass
ψ	yaw angle of the complete vehicle

Subscripts

1, 2, 3, 4	front-left, front-right, rear-left, rear-right
a	accumulator
B	bottom
f	front
H	hydraulic
int	internal
M	mechanical
p	pre-charge
r	rear
s	sprung mass
T	top
u	unsprung mass
v	damper valve
$x/y/z$	reference to one of the vehicle axes

References

[1] NHTSA, *Traffic Safety Facts*, National Highway Traffic Safety Administration, 2004.

[2] M.C. Smith and G.W. Walker, *Interconnected vehicle suspension*, Proc. Inst. Mech. Eng. D, J. Automob. Eng. 219 (2005), pp. 295–307.

[3] A.E. Moulton and A. Best, *Hydragas suspension*, SAE Technical Paper Series, SAE 790374, 1979.

[4] J.R. Wilde, G.J. Heydinger, and D.A. Guenther, *ADAMS simulation of ride and handling performance of the kinetic suspension system*, SAE Technical Paper Series, SAE 2006-01-1972, 2006.

[5] J.R. Wilde, G.J. Heydinger, D.A. Guenther, T. Mallin, and A.M. Devenish, *Experimental evaluation of Fishhook maneuver performance of a kinetic suspension system*, SAE Technical Paper Series, SAE 2005-01-0392, 2005.

[6] D. Cao, S. Rakheja, and C.-Y. Su, *Comparison of roll properties of hydraulically and pneumatically interconnected suspensions for heavy vehicles*, SAE Technical Paper Series, SAE 2005-01-3593, 2005.

[7] D. Cao, S. Rakheja, and C.-Y. Su, *Pitch attitude control and braking performance analysis of heavy vehicle with interconnected suspensions*, SAE Technical Paper Series, SAE 2007-01-1347, 2007.
[8] D. Cao, S. Rakheja, and C.-Y. Su, *Property analysis of an X-coupled suspension for sport utility vehicles*, SAE Technical Paper Series, SAE 2008-01-1149, 2008.
[9] D. Cao, S. Rakheja, and C.-Y. Su, *Pitch plane analysis of a twin-gas-chamber strut suspension*, Proc. Inst. Mech. Eng. D, J. Automob. Eng. 222 (2008), pp. 1313–1335.
[10] P.J. Liu, S. Rakheja, and A.K.W. Ahmed, *Properties of an interconnected hydro-pneumatic suspension system*, Trans. Can. Soc. Mech. Eng. 19 (1995), pp. 383–396.
[11] P.J. Liu, S. Rakheja, and A.K.W. Ahmed, *An analytical study of an interconnected vehicle suspension*, presented at ASME International Mechanical Engineering Congress and Exposition, San Francisco, CA, 1995.
[12] N. Zhang, W.A. Smith, and J. Jeyakumaran, *Hydraulically interconnected vehicle suspension: Background and modelling*, accepted for publication in Veh. Syst. Dyn. 48(1) (2010), pp. 17–40.
[13] W. Smith, N. Zhang, and J. Jeyakumaran, *Ride simulations of a half-car with a hydraulically interconnected passive suspension*, FISITA-2006 World Automotive Congress, Japan, 2006.
[14] W. Smith and N. Zhang, *Experimental and theoretical investigation into the dynamics of a half-car with an interconnected passive suspension*, SAE Technical Paper Series, SAE 2009-01-0579, 2009.
[15] N. Zhang, G.-M. Dong, and H. Du, *Investigation into untripped rollover of light vehicles in the modified fishhook and the sine maneuvers. Part I: Vehicle modelling, roll and yaw instability*, Veh. Syst. Dyn. 46 (2008), pp. 271–293.
[16] H.B. Pacejka, *Tyre and Vehicle Dynamics*, SAE International, Warrendale, PA, 2002.
[17] Kinetic Pty Ltd, Company Website, *Cannonball Productions*, 2005. Available at http://www.kinetic.au.com (accessed 13 July 2008).
[18] F.G. Guzzomi, P.L. O'Neill, and A.C.R. Tavner, *Investigation of damper valve dynamics using parametric numerical methods*, presented at 16th Australasian Fluid Mechanics Conference, Gold Coast, Australia, 2007.
[19] G.J. Forkenbrock, W.R. Garrott, M. Heitz, and B.C. O'Harra, *An experimental examination of J-turn and Fishhook maneuvers that may induce on-road, untripped, light vehicle rollover*, SAE Technical Paper Series, SAE 2003-01-1008, 2003.
[20] M. Ortiz, *Principles of interconnected suspensions*, in *RaceCar Engineering*, Vol. 7, 1997.
[21] W.A. Smith, *An investigation into the dynamics of vehicles with hydraulically interconnected suspensions*, Ph.D. thesis, University of Technology, Sydney, 2009.
[22] W. Smith, N. Zhang, and J. Jeyakumaran, *High frequency parameter sensitivity in hydraulically interconnected suspensions*, Proceedings of the 5th Australasian Congress on Applied Mechanics (ACAM), Brisbane, Australia, 10–12 December, 2007.
[23] J. Zhao and N. Zhang, *Vibration of hydraulically interconnected suspensions due to fluid-structure interaction*, Proceedings of the 13th Asia-Pacific Vibration Conference, University of Canterbury, Christchurch, New Zealand, 22–25 November, 2009.